One-Pot Synthesis of Highly Crystallined λ-MnO2 Nanodisks Assembled from Nanoparticles: Morphology Evolutions and Phase Transitions

ARTICLE *in* THE JOURNAL OF PHYSICAL CHEMISTRY C · DECEMBER 2007

Impact Factor: 4.77 · DOI: 10.1021/jp0743875

8 AUTHORS, INCLUDING:

Lin He
Beijing Normal University
117 PUBLICATIONS **1,193** CITATIONS
SEE PROFILE

Wei Zhang
Argonne National Laboratory
36 PUBLICATIONS **257** CITATIONS
SEE PROFILE

Chinping Chen
Peking University
96 PUBLICATIONS **1,662** CITATIONS
SEE PROFILE

Rongming Wang
University of Science and Technology Beijing
169 PUBLICATIONS **4,426** CITATIONS
SEE PROFILE

One-Pot Synthesis of Highly Crystallined λ-MnO_2 Nanodisks Assembled from Nanoparticles: Morphology Evolutions and Phase Transitions

Ning Wang,[†] Xia Cao,[†] Lin He,[‡] Wei Zhang,[‡] Lin Guo,*[,†,||] Chinping Chen,*[,‡] Rongming Wang,[§] and Shihe Yang*[,||]

School of Materials Science and Engineering, Beijing University of Aeronautics and Astronautics, Beijing, 100083, China, Department of Physics, Peking University, Beijing 100871, China, School of Science, Beijing University of Aeronautics and Astronautics, Beijing, 100083, China, and Department of Chemistry, The Hong Kong University of Science and Technology, Clear Water Bay, Kowloon, Hong Kong, China

Received: June 6, 2007; In Final Form: September 13, 2007

Manganese oxides are important materials in many applications. We describe, for the first time, the facile one-pot synthesis of highly crystallined λ-MnO_2 nanodisks assembled from nanoparticles through a novel wet chemical route. Morphology evolutions, magnetic properties, and phase transitions are also studied by transmission electron microscopy, scanning electron microscopy and thermal gravimetric analysis. A mechanism for the formation of the λ-MnO_2 nanodisks as well as their inner structure is proposed based on controlled experiments. The key to the successful preparation of this novel MnO_2 nanostructure has been a synergic control of a surfactant, polyvinylpyrrolidone, and a solvent, dimethyl sulfoxide, capable of stabilizing the microreactors and promoting the assembly of manganese nanoparticles.

Introduction

Controlled fabrication of nanostructures is not only of scientific interest but also could produce real benefits for technological applications that derive from their peculiar and fascinating properties, superior to the corresponding bulk counterparts.[1] In general, crystalline structure and size of nanomaterials are important elements in determining their physical and chemical properties;[2] thus, rational control over these elements has become a hot topic in recent material research fields.[3]

Manganese oxides are important materials in many applications such as catalysts, electrodes, sensors, and magnetic materials.[4] As an important functional metal oxide, manganese dioxide is one of the most attractive inorganic materials because of its physical and chemical properties and wide applications in catalysis, ion exchange, molecular adsorption, biosensor, and, particularly, energy storage.[5]

It is well-known that manganese dioxide can exist in different structural forms, α-, β-, γ-, and λ-types, when the basic structure unit (namely, the [MnO_6] octahedron) is linked in different ways. Much effort has been directed toward the preparation of low-dimensional MnO_2 nanostructures with controlled morphologies. For example, α-, β-, and γ-MnO_2 were prepared in different morphologies, such as rods, wires, tubes, etc., using hydrothermal and other techniques.[6,7]

In this paper, we present a novel solution-phase synthesis route for the first growth of well-oriented and crystallized λ-MnO_2 nanodisks using polyvinylpyrrolidone (PVP) as the modifying and protecting agent. The novelty of this work is characterized by a one-pot procedure that combines formation of a nanoparticle precursor, 2D assembly, phase transformation, and disk shaping and that is easily controlled under mild conditions. In addition, the unique magnetic properties of these novel nanodisks are also reported.

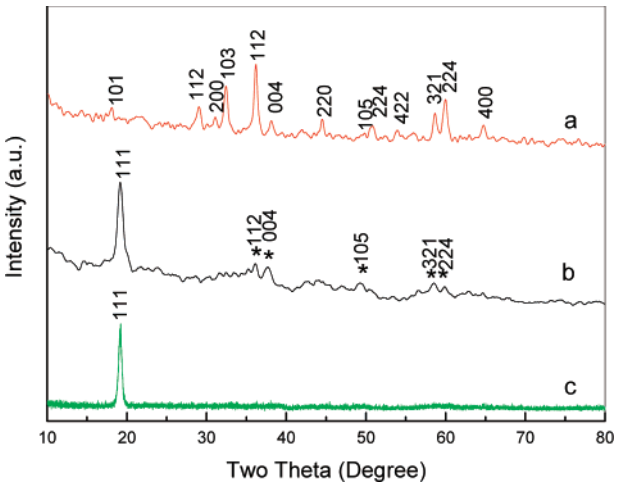

Figure 1. X-ray diffraction pattern of the as-prepared MnO_2 samples: (a) products at the initial stage of reflux, (b) products refluxed for 12 h, and (c) final products refluxed for 24 h.

Experimental Section

Synthesis of λ-MnO_2 Nanodisks. In a typical synthesis, MnO_2 nanodisks were prepared as follows: In brief, 1.4 g of $Mn(Ac)_2 \cdot 4H_2O$ and 2.0 g of PVP (MW 40 K) were added to 150 mL of dimethyl sulfoxide (DMSO). After 10 min of agitation and post-treatment with untrasonication, a mixture of 5 mL of hydrazine hydrate predissolved in 20 mL of ethanol was introduced slowly. Samples were taken out after the mixture was refluxed for about 1, 12, 24 h, respectively, and the final

* To whom correspondence should be addressed. E-mail: guolin@buaa.edu.cn. Tel: 86-10-82338162. Fax: 86-10-82338162.
[†] School of Materials Science and Engineering, Beijing University of Aeronautics and Astronautics.
[‡] Peking University.
[§] School of Science, Beijing University of Aeronautics and Astronautics.
[||] The Hong Kong University of Science and Technology.

10.1021/jp0743875 CCC: $40.75
Published on Web 12/19/2007

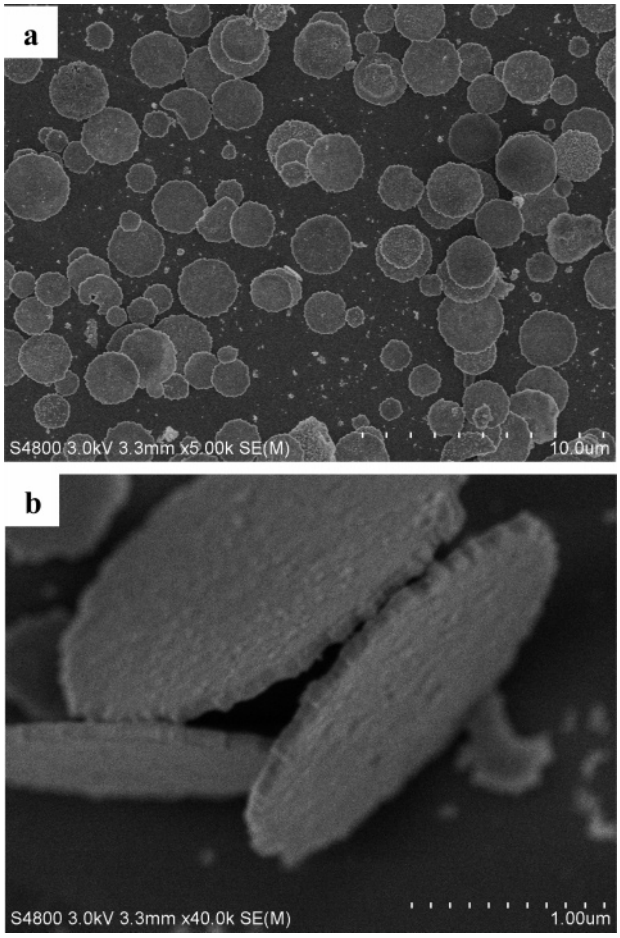

Figure 2. CFESEM images of the as-prepared λ-MnO_2 nanodisks. The magnifications of selected tiptoe zones: (a) 5 K; (b) 40 K.

products in the form of loose golden powder were obtained by centrifugation. The powder was rinsed repeatedly with absolute ethanol and water over six times and was followed by the removal of the residual solvent through evaporation in a vacuum at 333 K. All the reagents used in the experiments were of analytical grade (purchased from Beijing Chemical Industrial Co.) and used without further purification.

Synthesis of MnO_x Nanodisks. The conversion of the λ-MnO_2 to MnO_x nanodisks was carried out in an oven in air for 3 h at 573, 823, 1073, and 1273 K, respectively.

Characterization. The X-ray powder diffraction (XRD) pattern of the as-prepared products was collected by a Rigaku X-ray diffractometer (Rigaku Goniometer PMG-A2, CN2155D2, wavelength = 0.15147 nm) with Cu Kα radiation. Transmission electron microscopy (TEM) and scanning electron microscopy images were obtained by employing a JEOL JEM-2100F transmission electron microscope and a Hitachi S4800 cold-field emission scanning electron microscope (CFESEM). The thermogravimetric differential thermal analysis (TG-DTA) curve for heating the as-prepared λ-MnO_2 nanodisks was conducted by using a Perkin-Elmer Diamond TG-DTA system.

Results and Discussion

The XRD pattern of the as-prepared samples (Figure 1c) shows only a sharp (111) diffraction peak at 19.16° (full width at half-maximum $\approx$ 0.3°), which matches well with Bragg reflections of the standard λ-MnO_2 (*Fd*3*m*, a = 0.803 nm, JCPDF no. 44-0992). The absence of other peaks implies the highly preferential growth of MnO_2 nanodisks with high-quality

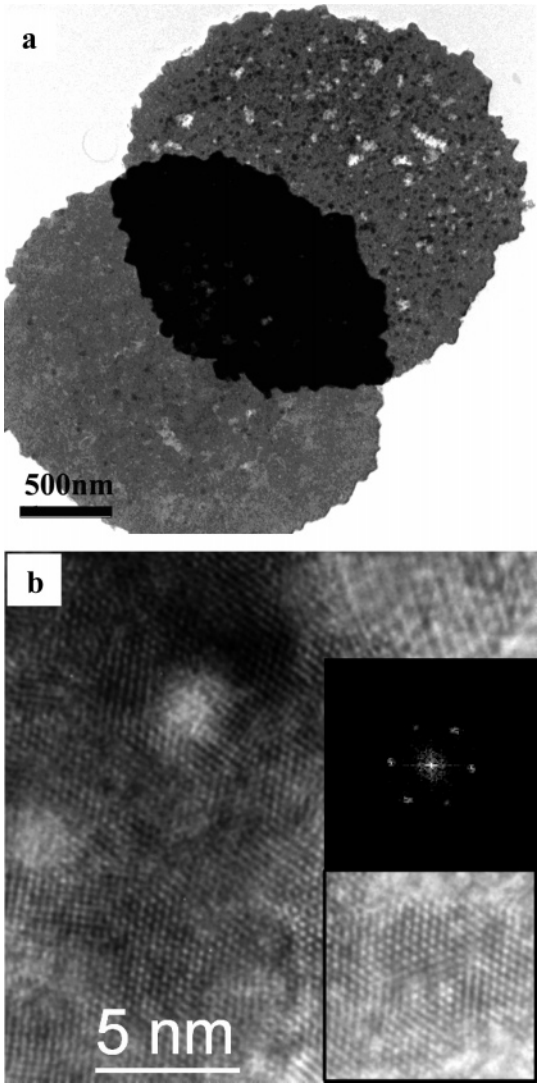

Figure 3. TEM and HRTEM images of the as-prepared λ-MnO_2 nanodisks.

crystalline. Figure 1a is the XRD pattern of the products at the initial stage (refluxed for 2 h), which can be indexed to Mn_3O_4 ($I4_1/amd$, a = 5.765, c = 9.442 JCPDF no. 75-1560); this demonstrates that the λ-MnO_2 nanodisks may result from Mn_3O_4 nanoparticles. Figure 1b shows the XRD pattern of the samples (refluxed for 12 h). It can be seen that λ-MnO_2 has already been obtained at this stage, while other minor phases (Mn_3O_4, denoted with star) still coexisted. Only after a long reflux time (>24 h) was the final crystallographic orientation obtained, which has a largely enhanced (111) diffraction peak that suppresses the other peaks too weak to be detected. In our viewpoint, the enhanced (111) peak may be partly due to the texture that the disks lay down on the supporting substrate. Since the disks are (111) oriented, XRD will only detect (111) and its multiples.

As can be seen in Figure 2, the products consist of relatively uniform λ-MnO_2 circular nanodisks mostly with a size of 1−2 μm. The detailed information on the nanodisks can be obtained in Figure 2b. From these higher-magnification SEM images of selected tiptoe zone, it can seen that the thicknesses of these disks are in the range of 50−100 nm, mainly about 60 nm. The surfaces of these disks are smooth, and the nanodisks display high regularity and yield well-ordered crystalline. The complex structures are sufficiently stable and are kept unchanged even after long ultrasonication time.

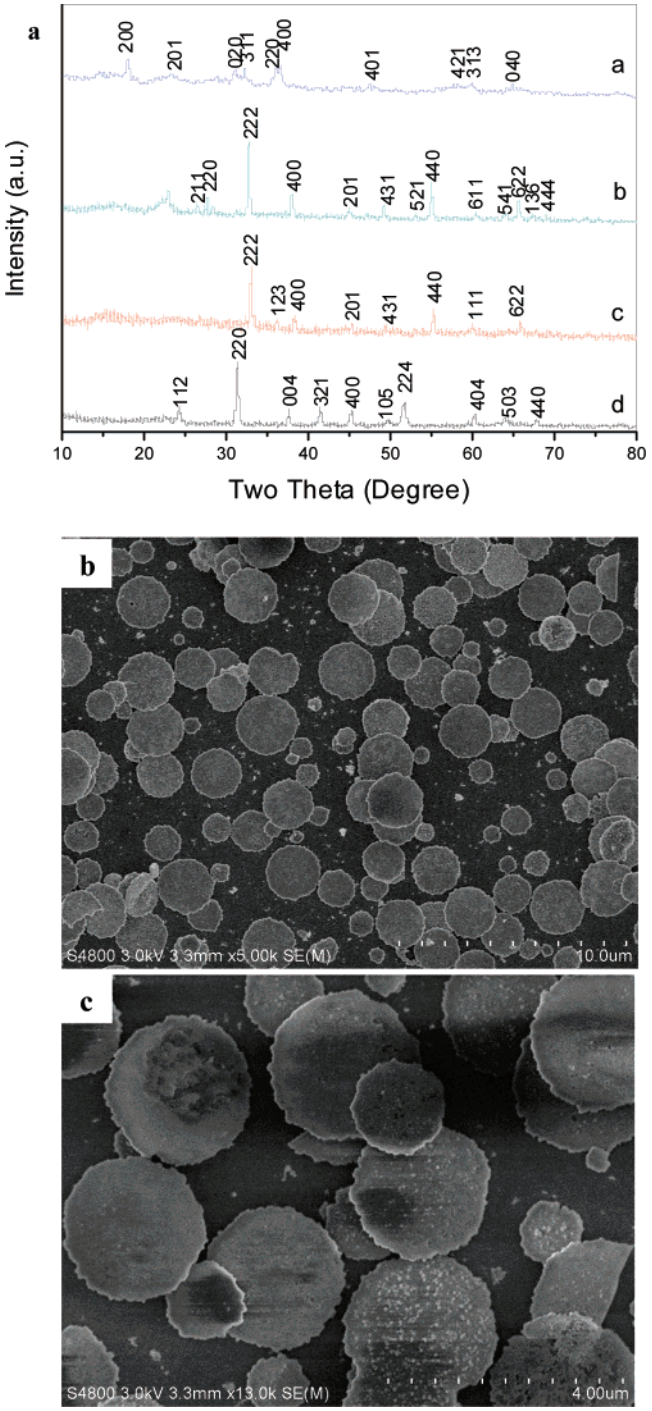

Figure 4. XRD patterns of the MnO_x nanodisks calcinated at (a) 573 K, (b) 823 K, (c) 1073 K, and (d) 1273 K (a) and SEM images of the MnO_x nanodisks calcinated at 1298 K (b and c).

Figure 3a is a typical as-prepared sample's TEM image. It shows that the sample's diameter is about 2 μm. High-resolution TEM (HRTEM) also enabled the viewing of lattice fringes, confirming crystallinity of the nanodisks. The vague boundaries among particles at the surface implicate a growth mechanism of particle attachment. As shown in Figure 3b, the HRTEM image of the λ-MnO_2 nanodisks is determined to grow along the [111] zone axis. The lattice fringe spacings are measured to be 0.28 nm, matching the d value for λ-MnO_2 (220) planes (0.284 nm). The inset is a Fourier transform of the image marked by the black square, indicating that the nanodisk is viewed along the [111] zone axis of the cubic structure. Irregularities can also

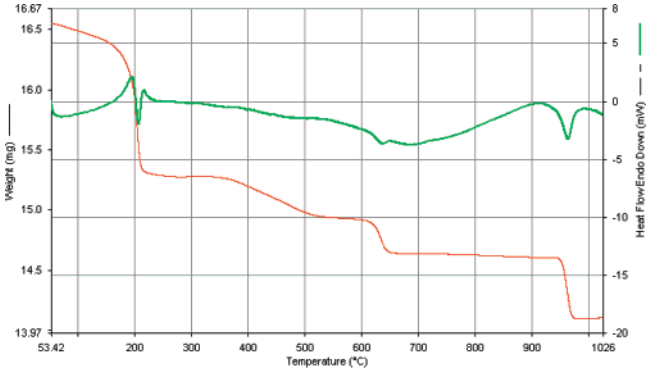

Figure 5. TG-DTA curve for heating the as-prepared λ-MnO_2 nanodisks from 298 to 1298 K.

be seen on the edge, which may imply a radial growth mechanism, that is, from center to radial.

Further calcinations of λ-MnO_2 nanodisks under different temperatures (573, 823, 1073, and 1273 °C) yielded pure-phase Mn_5O_8 (*C*2/*m*, $a = 1.034$ nm, $b = 0.5724$ nm, $c = 0.4852$ nm, JCPDF no. 72-1427), Mn_2O_3 ($P2_13$, $a = 0.9410$ nm, JCPDF no. 76-0150), Mn_2O_3 (*Ia*/3, $a = 0.9409$ nm, JCPDF no. 41-1442), and Mn_3O_4 (*I*41/*amd*, $a = 0.8140$ nm, $c = 0.942$ nm, JCPDF no. 75-1560), respectively. Inset a−d of Figure 4a show the XRD patterns of the manganese oxides obtained after calcinations, all peaks in each pattern can be well indexed to the corresponding JCPDF number mentioned above. The SEM image of the Mn_3O_4 products obtained after calcination under 1273 K, the highest temperature used here, is shown in parts b and c of Figure 4. It can be seen that the biscuitlike structure was basically maintained even after long time calcinations at 1273 K. No obvious collapse due to the shrinkage was found, and the nanodisk dimension was indeed almost the same as that before calcination.

Figure 5 shows a differential scanning calorimetry scan of the λ-MnO_2 nanodisks heated from 298 to 1298 K. Two sharp peaks appear at temperatures ranging from 423 to 473 K, due to the phase transition from λ-MnO_2 to Mn_5O_8. The broad peak ranging from 623 to 773 K results from the decomposition of Mn_5O_8 to Mn_2O_3, which is consistent with the XRD results. Though it has been proven that the products λ-MnO_2 calcinated at 823 and 1073 K are all Mn_2O_3, their lattice constants inferred from the XRD patterns are slightly different, which may be responsible for the DTA peak within the range of 873 to 923 K. It can be deduced that some phase transition has happened here. The sharp peak at 1223 K can be easily ascribed to the transition from Mn_2O_3 to pure-phase Mn_3O_4.

Time-dependent experiments were also carried out to further investigate the growth mechanism of the nanodisks. As can be noted from the synthesis procedure, in the initial stage of refluxing, only dispersed Mn_3O_4 nanoparticles appeared (Figures 1a, 6a, and 6d), which proved that the initial nucleated Mn_3O_4 particles are the original material sources for subsequent particle aggregations. With the elongation of reaction time, the Mn_3O_4 particles tended to assemble with each other, forming sheetlike patterns (parts b and e of Figure 6). This phenomenon may be partly caused by the reaction environment, which promotes the surface domains on neighboring nanoparticles to match up by aligning their magnetic moments during the refluxing process. In addition, for the formation of such nanodisks, the oligomerization of manganese oxylate must be another key step, a process that has been well discussed in many publications for the same or similar metal alkoxides.[8] That is, in the initial stage of refluxing, as refluxing was continued, through the formation

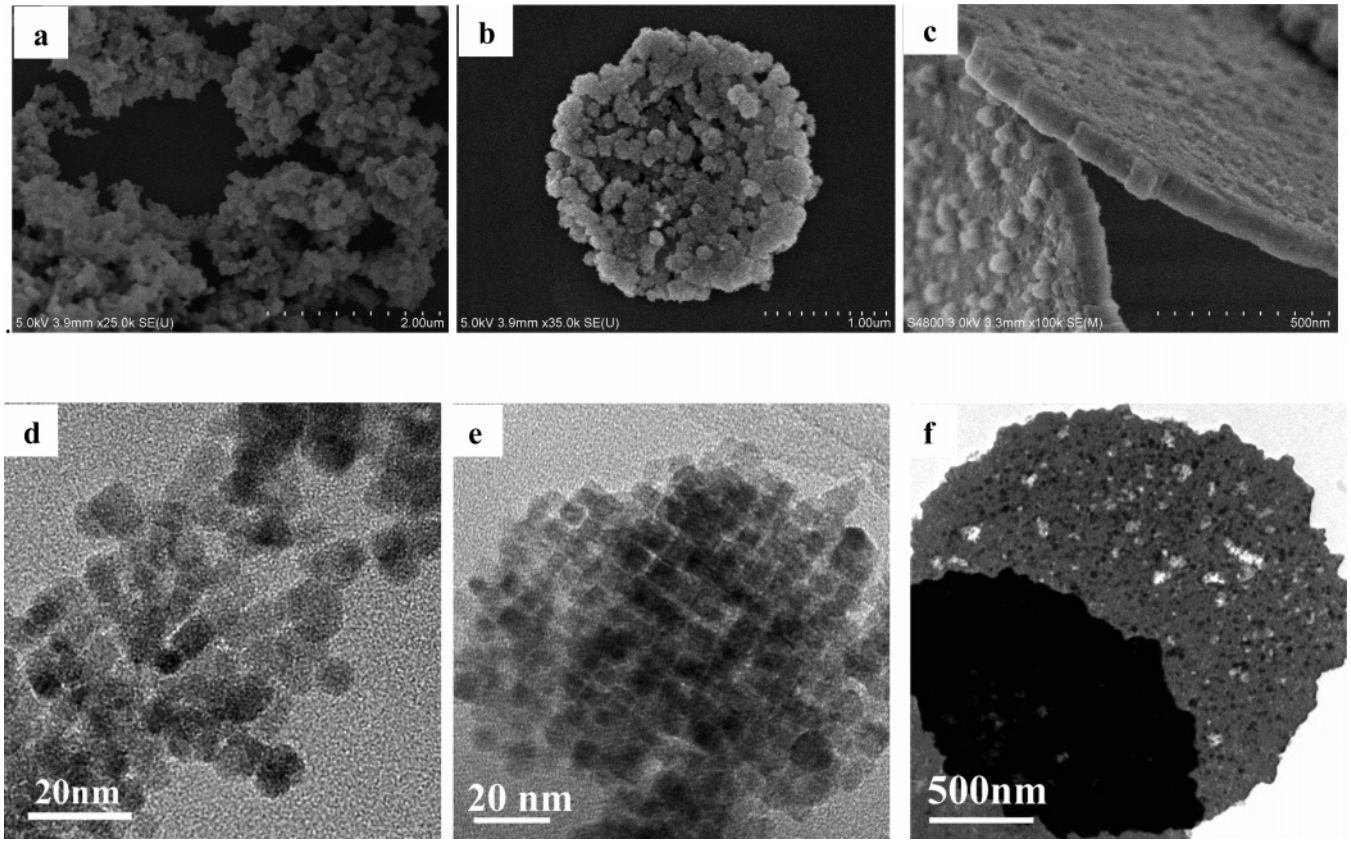

Figure 6. SEM (a−c) and TEM (d−f) images of the products at different stages. (a and d) Mn_3O_4 aggregates at the initial stage of reflux; (b and e) intermediate product; (c and f) λ-MnO_2 nanodisk (after refluxing for 24 h).

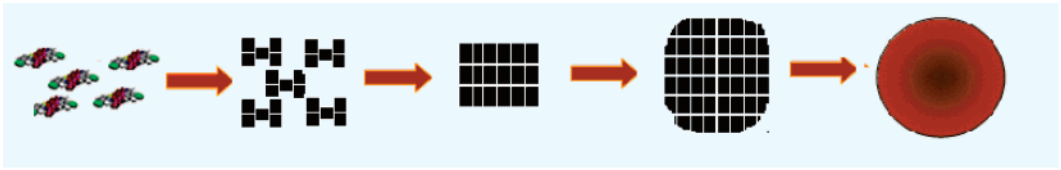

Figure 7. Schematic illustration of a proposed mechanism responsible for the formation of the nanodisks.

of Mn−O− covalent and Mn←OH coordination bonds, the manganese oxylates tended to form longer chains, which could further self-assemble into ordered bundles (nanochains) through van der Waals interactions. Here the metal salt generally remained as Mn(II) in the precursor nanopatterns.[9] The particle aggregates and growth at the intermediate stage (Figure 6b) are generally attributed to the traditional colloidal theory, the Ostwald ripening process; the diameters of the nanoparticle observed within the nanodisks developed visibly while the refluxing process continued. Besides this, for the formation of nanodisks with diameters well over 1000 nm and thickness no more than 80 nm, the directional effects of a capping agent such as DMSO and PVP are indispensable for the oriented particle attachment where Mn_3O_4 nanocrystals serve as "building blocks" while reducing the total surface energy through eliminating the higher surface energy faces.[9] Thus with the help of directional effects of capping agents DMSO and PVP, the particle attached disks were finally oxidized to MnO_2. On the basis of the above-mentioned time-dependent crystallinity and morphology evolution, a schematic illustration of the proposed particle attachment growth mechanism responsible for the formation of the nanodisks is listed in Figure 7.

Conclusions

We conclude that highly crystallined λ-MnO_2 nanodisks can be obtained by a simple solution-phase synthesis method at low temperatures. The in situ precipitation of the Mn salt results in Mn_3O_4 precursors. By thermally activated treatment of the precursor-containing solution, the time-dependent highly preferential growth of MnO_2 nanodisks will be sluggishly generated. To our best knowledge, there is no report on the novel preparation of λ-MnO_2 nanodisks crystal with high orientation. The plane surface being perpendicular to the *z*-axis dominantly can form an interface with other media, thus giving us the concrete image regarding the properties of MnO_2 nanodisks. The as-prepared λ-MnO_2 nanodisks can be further transited to Mn_5O_8, Mn_2O_3, and Mn_3O_4 by calcination while maintaining their initial biscuitlike nanostructure. This synthesis route is easily controllable, repeatable, mild, and feasible to apply to the fabrication of nanostructures of other materials. A corresponding mechanism of the formation of disklike crystals is tentatively suggested. These high-quality λ-MnO_2 nanodisks represent a new platform for further studies of nanoscale phenomena as well as for applications in various fields of nanotechnology.

Acknowledgment. This project was financially supported by National Natural Science Foundation of China (20673009, 20725208 and 50671003), the Program for New Century Excellent Talents in University (NCET-04-0164 and 06-0175), as well as the National Basic Research Program of China (2006CB932300). Support from the Research Grants Council of Hong Kong (604206) are also acknowledged.

References and Notes

(1) (a) Nalwa, H. S. *Handbook of Nanostructured Materials and Nanotechnology*; Academic Press: New York, 2000. (b) Burda, C.; Chen, X. B.; Narayanan, R.; El-Sayed, M. A. *Chem. Rev.* **2005**, *105*, 1025−1102.

(2) Alivisatos, A. P. *Science* **1996**, *271*, 933−937.

(3) Xia, Y.; Yang, P.; Sun, Y.; Wu, Y.; Mayer, B.; Gates, B.; Yin, Y.; Kim, F.; Yan, H. *Adv. Mater.* **2003**, *15*, 353−398.

(4) (a) Li, J.; Wang, Y. J.; Zou, B. S.; Wu, X. C.; Lin, J. G.; Guo, L.; Li, Q. S. *Appl. Phys. Lett.* **1997**, *70*, 3047−3049. (b) Kim, S. H.; Kim, S. J.; Oh, S. M. *Chem. Mater.* **1999**, *11*, 557−563. (c) Tang, W. P.; Kanoh, H.; Yang, X. J.; Ooi, K. *Chem. Mater.* **2000**, *12*, 3271−3279. (d) Lee, Y. J.; Grey, C. P. *J. Phys. Chem. B* **2002**, *106*, 3576−3582. (e) Lee, G. H.; Huh, S. H.; Jeong, J. W.; Choi, B. J.; Kim, S. H.; Ri, H.-C. *J. Am. Chem. Soc.* **2002**, *124*, 12094−12095. (f) Omomo, Y.; Sasaki, T.; Wang, L. Z.; Watanabe, M. *J. Am. Chem. Soc.* **2003**, *125*, 3568−3575. (g) Stobbe, E. R.; de Boer, A. A.; Geus, J. W. *Catal. Today* **1999**, *47*, 161−167. (h) Tarascon, J. M.; Armand, M. *Nature* **2001**, *414*, 359−367. (i) Shen, Y. F.; Zerger, R. P.; De Guzman, R. N.; Suib, S. L.; McCrudy, L.; Potter, D. I.; O'Young, C. L. *Science* **1993**, *260*, 511−515. (j) Giraldo, S. L.; Brock, W. S.; Willis, M.; Marquez, S. L.; Suib, S. L. *J. Am. Chem. Soc.* **2000**, *122*, 9330−9331.

(5) (a) Chabre, Y.; Pannetier, *J. Prog. Solid State Chem.* **1995**, *23*, 1−130. (b) Thackeray, M. M. *Prog. Solid State Chem.* **1997**, *25*, 1−28. (b) Espinal, L.; Suib, S. L.; Rusling, J. F. *J. Am. Chem. Soc.* **2004**, *126*, 7676−7682. (c) Chitrakar, R.; Kanoh, H.; Kim, Y. S.; Miyai, Y.; Ooi, K. *J. Solid State Chem.* **2001**, *160*, 69−76. (d) Armstrong, A. R.; Bruce, P. G. *Nature* **1996**, *381*, 499−500. (e) Ammundsen, B.; Paulsen, J. *Adv. Mater.* **2001**, *13*, 943−956. (f) Winter, M.; Brodd, R. J. *Chem. Rev.* **2004**, *104*, 4245−4270. (g) Toupin, M.; Brousse, T.; Bélanger, D. *Chem. Mater.* **2002**, *14*, 3946−3952.

(6) (a) Wang, X.; Li, Y. D. *Chem.−Eur. J.* **2003**, *9*, 300−306. (b) (23) Wang, X.; Li, Y. D. *J. Am. Chem. Soc.* **2002**, *124*, 2880−2881. (c) Xiong, Y. J.; Xie, Y.; Li, Z. Q.; Wu, C. Z. *Chem.−Eur. J.* **2003**, *9*, 1645−1651. (d) Wei, M.; Konishi, Y.; Zhou, H.; Sugihara, H.; Arakawa, H. *Nanotechnology* **2005**, *16*, 245−249. (e) Yuan, Z. Y.; Ren, T. Z.; Du, G. H.; Su, B. L. *Appl. Phys. A* **2005**, *80*, 743−747. (f) Zheng, D.; Sun, S.; Fan, W.; Yu, H.; Fan, C.; Cao, G.; Yin, Z.; Song, X. *J. Phys. Chem. B* **2005**, *109*, 16439−16443. (g) Sasaki, T.; Kumagai, N.; Komaba, S. *Electrochemistry* **2004**, *72*, 688−693.

(7) Cheng, F. Y.; Chen, J.; Gou, X. L.; Shen, P. W. *Adv. Mater.* **2005**, *17*, 2753−2756.

(8) (a) Fenton, D.; Gould, R.; Harrison, P.; Harvey, T.; Omietanski, G.; Sze, C. Zuckerman, *J. Inorg. Chim. Acta* **1970**, *4*, 235−239. (b) Cocks, G. Zuckerman, *J. Inorg. Chem.* **1965**, *4*, 592−597. (c) Honnick, W.; Zuckerman, *J. Inorg. Chem.* **1978**, *17*, 501−504. (d) Korb, G.; Levy, G.; Brini, M.; Deluzarche, A. *J. Organomet. Chem.* **1970**, *23*, 437−443. (e) Pommier, J.; Valade, J. *J. Organomet. Chem.* **1968**, *12*, 433−442. (f) Pommier, J.; Mendes, E.; Valade, J. *J. Organomet. Chem.* **1973**, *55*, C19. (g) Murakami, Y.; Matsumoto, T.; Yahikozawa, K.; Takasu, Y. *Catal. Today* **1995**, *23*, 383−389. (h) Mehrotra, R.; Gupta, V. *J. Organomet. Chem.* **1965**, *4*, 151−156. (i) Gaur, D.; Srivastava, G.; Mehrotra, R. *J. Organomet. Chem.* **1973**, *47*, 95−102. (j) Bradley, D.; Mehrotra, R.; Gaur, D. *Metal Alkoxides*; Academic Press: London, 1978; Chapter 4. (k) Scott, R.; Coombs, N.; Ozin, G. *J. Mater. Chem.* **2003**, *13*, 969−974. (l) Russell, G.; Henrichs, P.; Hewitt, J.; Grashof, H.; Sandhu, M. *Macromolecules* **1981**, *14*, 1764−1770. (m) Barroso-Bujans, F.; Martinez, R.; Ortiz, P. *J. Appl. Polym. Sci.* **2003**, *88*, 302−306. (n) Yuliang, W.; Xuchuan, J.; Younan, X. *J. Am. Chem. Soc.* **2003**, *125*, 16176−16177.

(9) (a) Banfield, J. F.; Welch, S. A.; Zhang, H. Z.; Ebert, T. T.; Penn, R. L. *Science* **2000**, *289*, 751−754. (b) Liu, B.; Zeng, H. C. *J. Am. Chem. Soc.* **2004**, *126*, 8124−8125.